ACADÉMIE
DES SCIENCES
INSTITUT DE FRANCE

Comptes Rendus
Chimie

Abdelbasset Ben Dkhil, Haitham Elleuch, Anissa Somrani and Amor Hafiane

Efficient nitrate removal from water by biosorption onto a southern Mediterranean Sea native plant *Posidonia oceanica* (L.) powder

Volume 28 (2025), p. 705-726

Online since: 2 October 2025

https://doi.org/10.5802/crchim.412

The Comptes Rendus. Chimie *are a member of the Mersenne Center for open scientific publishing*
www.centre-mersenne.org — e-ISSN : 1878-1543

ACADÉMIE DES SCIENCES
INSTITUT DE FRANCE

Comptes Rendus. Chimie
2025, Vol. 28, p. 705-726
https://doi.org/10.5802/crchim.412

Research article

Efficient nitrate removal from water by biosorption onto a southern Mediterranean Sea native plant *Posidonia oceanica* (L.) powder

Abdelbasset Ben Dkhil [a,b,*], **Haitham Elleuch** [b,c], **Anissa Somrani** [b,d] **and Amor Hafiane** [a]

[a] Laboratory of Water, Membrane and Environmental Biotechnology LR15CERTE04, Center of Research and Water Technologies, University of Carthage, Technopole of Borj Cedria, PB 273, 8020 Soliman, Tunisia

[b] Department of Chemistry, Higher Institute of Sciences and Technologies of Environment, University of Carthage, Borj Cedria, P.B. no 1003, 2050 Hammam Lif, Tunisia

[c] Laboratory of Structural Organic Chemistry and Macromolecular LR99ES14, Faculty of Sciences of Tunis, University of Tunis El Manar, University Campus, 2092 Tunis, Tunisia

[d] Department of Physics, College of Science, Jouf University, Sakaka, Aljouf 72341, Saudi Arabia

E-mail: alwaysoptimist20@gmail.com (A. B. Dkhil)

Abstract. An efficient method for nitrate removal from water was developed using the sea plant *Posidonia oceanica* (L.) as a biosorbent. Never used previously for this purpose, this plant was applied in its natural form without any chemical modification or cross-linking with another material. The nitrate biosorption was carried out in batch experiment at room temperature and under the optimum conditions of agitation time, biosorbent dose, and pH. The Langmuir model fits the experimental biosorption isotherm data better than the Freundlich one, confirming a monolayer adsorption process onto homogeneous surface and giving a relatively high maximum biosorption capacity 41.6 $mg{\cdot}g^{-1}$ of nitrate nitrogen, thus demonstrating a good efficiency of the biosorbent. The thermodynamic study shows not only that the biosorption process is spontaneous and endothermic in nature, but also that increasing temperature enhances the nitrate uptake. Furthermore, the Dubinin–Radushkevich modeling gives a mean free energy of 15.81 $kJ{\cdot}mol^{-1}$, indicating that nitrate was chemisorbed. The same result was confirmed by kinetic modeling, which showed that the pseudo-second-order model fits the experimental data better than the pseudo-first order. The characterization by Fourier transform infrared spectroscopy (FTIR), scanning electron microscopy (SEM), and energy-dispersive X-ray spectroscopy (EDS) revealed that nitrate was mainly retained on the biosorbent surface through electrostatic forces with protonated amines (RNH_3^+; $R_2NH_2^+$ and R_3NH^+). However, ion exchange with hydroxide ions and intraparticle diffusion may play an important role in the biosorption process.

Keywords. Nitrate, Biosorption, *P. oceanica* (L.), Tunisian coasts, Ecophysiology, Isotherm modeling, Mechanism.

Funding. Ministry of Higher Education and Scientific Research of Tunisia.

Manuscript received 15 September 2024, revised 23 April 2025, accepted 24 July 2025.

* Corresponding author

1. Introduction

The most common inorganic nitrogen species in the environment are ammonia (NH_3 or NH_4^+), nitrite NO_2^- and nitrate NO_3^-. Ammonia is always oxidized to nitrate through two successive steps by nitrifying bacteria: (NH_3 or NH_4^+) $\rightarrow$ NO_2^- $\rightarrow$ NO_3^-. As a result, the nitrate concentration in water and soil is usually higher than that of other inorganic nitrogen species [1]. Nitrate and other inorganic nitrogen species are present in aquatic environments as normal biological degradation products of proteins and nucleic acids. They can also enter natural waters through agricultural fertilizers, animal excrement runoff, industrial wastes, and sewage effluents [2,3]. Due to its high solubility, nitrate is considered as one of the most common contaminants in the ground water aquifers destined for drinking water supplies [4]. In fact, the consumption of an excessive amount of nitrate can lead to some diseases, among which the most well-known is methemoglobinemia which affects bottle-fed infants under six months (blue baby syndrome) [5,6], and even children aged between one and seven years [7]. The latter study which was carried out in a North African country (Morocco) has shown that blue-baby syndrome affects about 36.2% of children who consume water with nitrate concentrations above 50 mg/L [7]. Incidentally, a study realized in Tunisia has revealed that groundwater in the north of the country significantly exceeds this concentration threshold [8].

Therefore, nitrate removal treatment of Tunisian groundwater is highly recommended to protect the child population. Furthermore, nitrate can be reduced to nitrite in acidic gastric medium, leading to the formation of nitrosamine compounds, which are suspected to cause gastric cancer among adult people [9]. A recent study conducted in Tunisia between 2010 and 2014 has demonstrated that stomach cancer rates are 61.4% in men and 38.6% in women. Among the most likely direct causes is the consumption of foods rich in nitrites and nitrates [10]. For this reason, the maximum admissible concentration level of nitrate in drinking water should not exceed 10 mg·L^{-1} of NO_3^- – N, as recommended by the World Health Organization (WHO) and the U.S. Environmental Protection Agency [11–14].

Furthermore, the nitrate ions have a direct impact on the environment, as a high input of nitrogen can cause a massive proliferation of phytoplankton and algae in the aquatic environments, leading to excessive consumption of dissolved oxygen. This phenomenon, called eutrophication, causes the death and decay of many aquatic organisms, causing in turn an imbalance of the ecosystem equilibrium [15,16]. Currently, the main treatment methods used for nitrate removal from natural water are reverse osmosis, electrodialysis, ion exchange, biological processes, and adsorption. Not only have these methods proven to be efficient, but they also provide high-quality water and some of them are easy to apply. However, some are relatively expensive, require high energy consumption and can be difficult to implement. Moreover, some generate large volumes of wastewater, which presents an additional challenge to address [17–23]. The adsorption method is based on the surface retention of nitrate ions via ionic bonds or by intraparticle diffusion on a finely divided solid material.

Compared to existing processes, adsorption is lower in cost, more easily applied, cleaner, and safer without releasing nitrate-laden wastewater or other chemicals. Currently, there is a wide range of adsorbents used to remove nitrate from water which could be natural or synthetic [24]. Natural adsorbents were used either in their native state without any modification of surface structure such as chitosan [25], sugarcane bagasse [26], agriculture waste [27] and algae [28], or thermally or chemically activated such as activated carbon derived from pomegranate rind, or [29] sepiolite activated by HCl [30], etc. The synthetic nitrate adsorbents can include polymer cross-linked with natural materials [31], activated materials coated with metal oxide nanoparticles [32], or chemical compounds cross-linked with a polymer [33]. The maximum adsorption capacity of nitrate, obtained with the adsorbents currently used, ranges from 0.25 to 350 mg·g^{-1} of nitrate nitrogen according to the experimental conditions in which the retention was carried out [24]. However, the yield and effectiveness of an adsorbent can be better evaluated objectively at the level of large-scale treatment station, where a large amount of this material will be needed and high volume of water will be treated. Consequently, the cost of the adsorbent will be a leading factor which determines

the economic profitability of the denitrification process.

Thus, due to the aforementioned reasons and within this context, the present research work tries to investigate a natural low-cost adsorbent for nitrate removal from aqueous solutions in batch experiments. The adsorbent applied is a sea plant *Posidonia oceanica* (L.) widely abundant on Mediterranean coasts and available almost throughout the year [34]. Apart from its nitrate biosorption properties in its dead state, the living *P. oceanica* plays an important role as a bioindicator for monitoring water quality, as well as for assessing ecosystem health and evaluating the impacts of climate change. In fact, *P. oceanica* meadows stabilize the sediment, protect the beaches from erosion and have a positive effect on the clarity of water [35–37]. As they are highly sensitive to anthropogenic effects, the long-term decline in shoot density and the morphological changes observed in *P. oceanica* meadows over several decades, indicate climate change driven by the environmental pollution [38–41].

In the present work, the biosorbent was used in a dead state. It was dried at room temperature, chipped and crushed into fine powder. The method shows good efficiency, requires no chemicals except a few drops of HCl or NaOH for pH adjustment, and does not release any waste effluent, making it a promising alternative denitrification process suitable for large-scale applications. Unlike reverse osmosis, electrodialysis, ion exchange, and biological denitrification, the adsorption process by *P. oceanica* requires neither pretreatment of raw water except pH adjustment nor posttreatment of water. This minimizes the treatment cost and increases the competitivity of the process in comparison to other denitrification processes cited previously. Furthermore, *P. oceanica* is organic matter that can be incinerated after use and preserved in a narrow place far from natural water resources, contributing to the environmental protection.

2. Material and methods

2.1. *Biosorbent preparation*

The seagrass *P. oceanica* was collected in the dead state as a ball of rolled-up brown fibers from the Soliman delegation beach, southeast of Tunis (GPS: Latitude: 30.732394, Longitude: 10.469454). The harvest was done at the beginning of summer, in June. The contribution of nitrates in this beach comes mainly from two sources: the discharge of urban water treated by a plant that does not carry out tertiary denitrification treatment and the runoff towards the sea of the excrement of cows which are very numerous in this region. A mass of 100 g of sea plant was put in 500 mL of distilled water and stirred during 24 h. Subsequently, the plant was dried at 80 °C, chipped and crushed. The surface area of *P. oceanica* powder was 25.75 $m^2 \cdot g^{-1}$ according to the Brunauer–Emmett–Teller (N_2-BET) isotherm method and using an Anton Pear autosorb 6100 analyzer. The powder obtained from the plant was transferred into a concentrated NaOH solution (1 M) and the mixture was stirred during 24 h [42–45]. The purpose of this operation is to force an ionic exchange between hydroxide ions (OH^-) and the nitrate ions (NO_3^-) already accumulated by the *Posidonia* fibers when it was in the sea. This ionic exchange could also clear *P. oceanica* of other anions such as: Cl^-, F^-, I^-, SO_4^-, etc., some of which disturb the determination of nitrate by the sodium salicylate method [46] and compete with it on the active sites of the biosorbent. Eventually, the biosorbent powder was washed with deionized water in excess, dried at 40 °C in an oven, and preserved in a desiccator for further use.

2.2. *Reagents*

All chemicals used were of analytical grade and all nitrate concentrations were expressed in nitrate nitrogen, such as 1 $mg \cdot L^{-1}$ of $NO_3^- - N$ corresponds to 4.428 $mg \cdot L^{-1}$ of NO_3^- [46]. The nitrate stock solution having a concentration of 100 $mg \cdot L^{-1}$ of $NO_3^- - N$ was prepared by dissolving 0.772 g of KNO_3 previously dried at 105 °C for 4 h, in pure water adjusted to a 1000 mL volumetric flask [1]. The stock solution was stored in a refrigerator at 4 °C and prepared anew every two months. Working standards ranging from 0.5 to 5 $mg \cdot L^{-1}$ of $NO_3^- - N$ were prepared immediately before usage by accurate serial dilution of the stock solution. The other solutions required for the nitrate calibration curve or to carry out the adsorption experiments were prepared by dissolving the corresponding salt in the appropriate volume of deionized water. The pH was adjusted using HCl or NaOH (0.1 M) solutions.

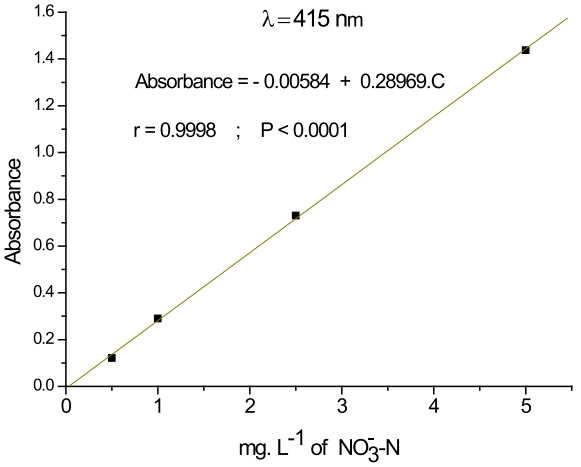

Figure 1. Calibration curve plotting absorbance versus concentration of standard solutions.

2.3. *Nitrate determination*

Nitrate concentration after each biosorption experiment was determined by the sodium salicylate spectrophotometric method described by many previous works [46–48]. Absorbance measurements were performed using a double beam Shimadzu 1800 UV–Vis spectrophotometer. Direct absorbance at 415 nm was recorded for each nitrate solution using a pair of UV quartz cells with 1 cm in optical path length. Nitrate concentration was deduced by the projection on a calibration curve plotting absorbance versus concentration. An example of such a calibration curve is given by Figure 1.

The linear fit of the points in Figure 1 gives a slope of 0.28958, an intercept of −0.00584 and a correlation coefficient of 0.9998. The latter parameter presents a strong linear correlation between absorbances and concentrations, confirming the accuracy of the nitrate determination method used.

2.4. *Batch biosorption experiments*

Batch experiment is an analytical method conducted in static mode, which involves contacting a fixed volume of water to purify in contact with a given mass of biosorbent, under controlled conditions of agitation time, temperature, and pH. For all experiments, the biomass dosage of *P. oceanica* was chosen at its optimum value and biosorption was conducted at room temperature (30 ± 2 °C), in 100 mL erlenmeyer flasks and under 100 rpm agitation. A given mass of *P. oceanica* was agitated in 30 mL of a nitrate solution using an LBX SO4X10 multiposition magnetic stirrer. The solution's pH was measured by an AZ 86505 pH meter and adjusted using HCl or NaOH (0.1 M) solutions as required. The zeta potential was determined using a Malvern S90 zetasizer.

2.5. *Biosorption isotherms*

Three isotherm models (Langmuir, Freundlich, and Dubinin–Radushkevich) were investigated to fit the sorption equilibrium data obtained in this research work. The comparison of the correlation coefficient (r) of the linear forms of all models indicates which isotherm provides the best fit of the experimental data and therefore best describes the sorption process.

The Langmuir isotherm describes quantitatively the formation of a monolayer adsorbate on the outer surface of the adsorbent, and no subsequent further adsorption takes place. This model assumes monolayer adsorption onto a homogeneous surface with a finite number of identical sites, and without interaction between sorbed molecules. Based on these assumptions, Langmuir established the equation of his model as follows (Equation (1)) [49,50]:

$$Q_e = \frac{Q_{max} b C_e}{1 + bC_e}, \tag{1}$$

where Q_e (mg·g^{-1}) is the amount of solute adsorbed by adsorbent at equilibrium, Q_{max} (mg·g^{-1}) is the maximum adsorption capacity, C_e (mg·L^{-1}) is the solute concentration at equilibrium and b (L·mg^{-1}) is the Langmuir constant related to the adsorption energy. The linear form is represented by the following equation:

$$\frac{1}{Q_e} = \frac{1}{Q_{max}} + \frac{1}{bQ_{max}C_e}. \tag{2}$$

The essential feature of the Langmuir isotherm may be expressed as a dimensionless equilibrium factor R_L, calculated as follows:

$$R_L = \frac{1}{1 + bC_0}. \tag{3}$$

The value of R_L indicates the adsorption nature to be unfavorable ($R_L > 1$), linear ($R_L = 1$), favorable ($0 < R_L < 1$), or irreversible ($R_L = 0$) [51]. The Freundlich isotherm is an empirical model based on the

adsorption on a heterogeneous surface and the adsorbate possibly multilayered. It is expressed by the following equation [50,52]:

$$Q_e = K_F C_e^{1/n}, \tag{4}$$

where K_F is the Freundlich constant indicative of adsorption capacity and n is a factor measuring the degree of heterogeneity of adsorption sites. The value of n indicates whether the adsorption is good ($2 < n < 10$), moderately difficult ($1 < n < 2$), or poor ($n < 1$) [53]. The linear form of this model is given as follows:

$$\mathrm{Ln}(Q_e) = \mathrm{Ln}(K_F) + \frac{1}{n}\mathrm{Ln}(C_e). \tag{5}$$

The Dubinin–Radushkevich (D–R) isotherm is generally applied to determine whether the nature of adsorption is physical or chemical. The D–R isotherm is more general than the Langmuir isotherm, as it is not based on ideal assumptions such as equipotential of the adsorption sites, the absence of steric hindrance between adsorbates and incoming particles, and surface homogeneity on a microscopic level [54,55]. The D–R isotherm gives insights into the adsorption mechanism based on potential theory and assuming a heterogeneous surface of the solid phase [55,56]. The linear form of the D–R isotherm is described by the following equation [57,58]:

$$\mathrm{Ln}(Q_e) = \mathrm{Ln}(Q_{max}) - \beta\varepsilon^2, \tag{6}$$

where Q_e (mol·g^{-1}) is the amount of solute retained by adsorbent at equilibrium, Q_{max} (mol·g^{-1}) the theoretical saturation capacity, β (mol^2·J^{-2}) an activity coefficient related to the mean free energy of adsorption and ε (J·mol^{-1}) is the Polanyi potential defined for the liquid/solid adsorption as follows [59]:

$$\varepsilon = RT\mathrm{Ln}\left(1 + \frac{1}{C_e}\right), \tag{7}$$

where R (8.314 J·mol^{-1}·K^{-1}) is the universal gas constant, T (K) the absolute temperature and C_e (mol·L^{-1}) the concentration of solute at equilibrium. The essential feature of the D–R isotherm is the mean free energy E (J·mol^{-1}), computed as follows:

$$E = \frac{1}{\sqrt{2\beta}}. \tag{8}$$

The value of E indicates whether the adsorption mechanism occurs as physisorption ($E < 8$ kJ·mol^{-1}) or chemisorption ($8 < E < 16$ kJ·mol^{-1}) [59,60]. Consistently with Equation (6), the plot $\mathrm{Ln}(Q_e)$ versus ε^2 allows the determination of β and Q_{max} through the slope and the intercept, respectively.

2.6. *Chi-square test*

The statistical hypothesis chi-square test (χ^2) is applied in this work to verify the conformity between the experimental data and the values predicted by a theoretical model. The comparison is made between the experimental equilibrium biosorption capacities and those calculated by the model.

The conformity chi-square test is based on two hypotheses, as follows:

Hypothesis H_0: There is conformity with the theoretical model at a given confidence level.

Hypothesis H_1: There is no conformity with the theoretical model.

The observed chi-square value is calculated as follows:

$$\chi^2_{obs} = \sum_{i=1}^{n} \frac{(Q_{e(exp)} - Q_{e(theo)})^2}{Q_{e(theo)}}, \tag{9}$$

where $Q_{e(exp)}$ and $Q_{e(theo)}$ are the experimental and calculated equilibrium biosorption capacities, respectively, n the number of measures, and $(n-1)$ the number of degrees of freedom.

The comparison between the observed chi-square value χ^2_{obs} and the critical chi-square value χ^2_c, at a given number of degrees of freedom and confidence level, can lead to two possibilities:

$\chi^2_{obs} \le \chi^2_c$: hypothesis H_0 is retained

$\chi^2_{obs} > \chi^2_c$: hypothesis H_1 is retained.

2.7. *Biosorption kinetic modeling*

In this research work, we applied the well-known and much-cited following kinetic models: pseudo-first order [61], pseudo-second order [62], and intraparticle diffusion models [63].

Table 1 shows the equation of each kinetic model and its integrated form, where Q_t and Q_e (mg·g^{-1}) are the amount of solute at an instant t (min) and at equilibrium, respectively, C_i (mg·g^{-1}) is a constant that depends on adsorbent nature, k_1 (min^{-1}), k_2 (g·mg^{-1}·min^{-1}), and k_p (mg·g^{-1}·min$^{-0.5}$) are the rate constant of the pseudo-first order, pseudo-second order, and intraparticle diffusion models, respectively. $Q_{cal.1}$ and $Q_{cal.2}$ are the calculated (theoretical) amounts of solute retained at adsorption equilibrium for the pseudo-first order and pseudo-second

order models, respectively. The coefficients k_1 and $Q_{cal.1}$, k_2 and $Q_{cal.2}$, and k_p can be estimated from the curve plotting $\mathrm{Ln}(Q_e - Q_t)$ versus t, t/Q_t versus t, and Q_t versus $t^{0.5}$ for the pseudo-first order, pseudo-second order, and intraparticle diffusion models, respectively (Table 1).

Among the first two models, the best fit was selected based on both linear regression correlation coefficient (r) of the plot and the concordance between the calculated and experimental equilibrium amount values (Q_e) of adsorbed solute. For the third model, the shape of the curve Q_t versus $t^{0.5}$ determines the importance of each transport step for solute adsorption.

2.8. *Thermodynamic parameters*

The thermodynamic parameters of the biosorption reaction such as equilibrium constant K_C, standard free enthalpy change ΔG_T^0, standard enthalpy ΔH_T^0 change and standard entropy change ΔS_T^0 were determined using the relations summarized in Table 2.

2.9. *Infrared spectroscopy analysis*

Infrared spectroscopy was used to determine the main functional groups in *P. oceanica* powder involved in the biosorption process. The powder of *P. oceanica* (3 mg) was dispersed in KBr (200 mg, spectroscopic grade), and the mixture was ground in an agate mortar until perfectly homogeneous. The mixture was transferred to a disc of diameter 1 cm under a pressure of 14 tons using a hydraulic press. The infrared spectra were recorded by scanning the range of 400–4000 cm^{-1} using a PerkinElmer Frontier FTIR spectrometer. The reference spectrum was a polystyrene film and the background spectrum of pure KBr was subtracted from the sample spectrum. Each recorded spectrum was the result of a ten-scan accumulation and was obtained with a 1 cm^{-1} spectral resolution.

Scheme 1 shows the two vibrational modes of nitrates that appear in the mid-infrared spectral region, whose corresponding bands could be very helpful in the characterization.

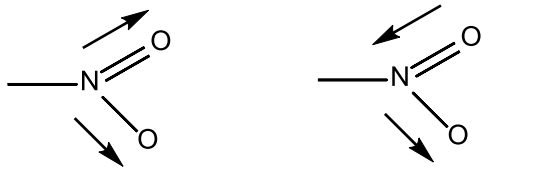

Scheme 1. Valence vibration of the nitro $-NO_2$ group.

2.10. *Analysis by scanning electron microscopy and energy dispersive spectroscopy*

The analysis by scanning electron microscopy (SEM) gives information about the topography change on the *P. oceanica* surface before and after nitrate biosorption. Likewise, the analysis by energy-dispersive X-ray spectroscopy (EDS) detects the slightest variation of chemical elemental composition of biosorbent surface. The two types of analysis were achieved by a ThermoFisher electron microscope at 100 and 10 µm resolution level, with 5 kV acceleration voltage, 500 µm horizontal field width and under a vacuum of 10^{-3} Pa.

3. Results and discussion

3.1. *Effect of experimental conditions*

3.1.1. *Effect of solution pH*

The initial pH is a crucial factor that should be taken into consideration in biosorption processes, as it provides information about the protonation state of active sites on the biosorbent surface and the possible influence of free hydronium ions (H_3O^+) and free hydroxide ions (OH^-) on the retention of nitrates. Firstly, the pH effect on zeta potential of water-suspended biosorbent is worth exploring to gain insight into its surface charge for each pH range. The zeta potential measurements of aqueous solutions containing suspended *P. oceanica* powder are displayed against pH in Figure 2. In pH ranging from 2 to 6, the zeta potential is positive with gradual decrease, thus confirming the presence of positively charged groups (RNH_3^+, $R_2NH_2^+$, R_3NH^+, and $-OH_2^+$) on the

Table 1. Original, linearized forms and deduced parameters of the kinetic models used

Kinetic model	Original form	Linearized form	Plot	Deduced parameters
Pseudo-first order model	$Q_t = Q_e(1-\exp(-k_1 t))$	$\mathrm{Ln}(Q_e - Q_t) = \mathrm{Ln}(Q_{cal.1}) - k_1 t$	$\mathrm{Ln}(Q_e - Q_t)$ versus t	Slope: k_1 Intercept: $Q_{cal.1}$
Pseudo-second order model	$Q_t = \dfrac{k_2 Q_t^2 t}{1 + k_2 Q_e t}$	$\dfrac{t}{Q_t} = \dfrac{1}{k_2 Q_{cal.2}^2} + \dfrac{1}{Q_{cal.2}} t$	$\dfrac{t}{Q_t}$ versus t	Slope: k_2 Intercept: $Q_{cal.2}$
Intraparticle diffusion model	$Q_t = k_p\sqrt{t} + C_I$	$Q_t = k_p\sqrt{t} + C_I$	Q_t versus t	Slope: k_p

Table 2. Thermodynamic relations used

Equilibrium biosorption constant	$K_C = \dfrac{(C_0 - C_e)}{C_e} = \dfrac{C_S}{C_e}$
Standard free enthalpy change	$\Delta G_T^0 = -RT\mathrm{Ln}(K_C) = \Delta H_T^0 - T \cdot \Delta S_T^0$
Van't Hoff relation	$\mathrm{Ln}(K_C) = \dfrac{\Delta S_T^0}{R} - \dfrac{\Delta H_T^0}{RT}$

Where C_e is the concentration of $NO_3^- - N$ ($mg{\cdot}L^{-1}$) at equilibrium and C_S the adsorbed concentration of $NO_3^- - N$ ($mg{\cdot}L^{-1}$) by biosorbent. The concentration C_S also represents the mass of adsorbate retained by adsorbent mass corresponding to one liter of solution [64].

biosorbent surface. The more neutralized the protonated groups are, the more the solution pH increases. Indeed, the rapid decrease in the zeta potential between pH = 6 and 6.5 can be attributed to the significant loss of positively charged groups neutralized by hydroxide ions. The zero-crossing point of the plot coincides with the pH value of 6.5. Commonly known as zero-charge point, this is when the surface of the biosorbent suspended in water is perfectly neutral, due to compensation between negative and positive charges on its surface. For pH values higher than the zero-charge point, the adsorbent surface becomes negatively charged due to the accumulation of hydroxide ions, which may cause the appearance of conjugate bases for some organic groups.

The pH effect on the biosorbed amount was investigated over the pH range from 2 to 12 and results are presented in Figure 3.

Three significant regions characterize the plot. The first one covers the pH acid range from 2 to 5 where the biosorption percentage tends to be constant with a slight variation between pH = 2 and 3. In this region, free H_3O^+ react with superficial functional groups of *P. oceanica* such as amine and alcohol and protonate them affording ionized functions RNH_3^+, $R_2NH_2^+$, R_3NH^+, and $-OH_2^+$, which retain nitrate (NO_3^-) by electrostatic forces. This result is in good agreement with the one obtained from the zeta potential study. However, at very low pH values

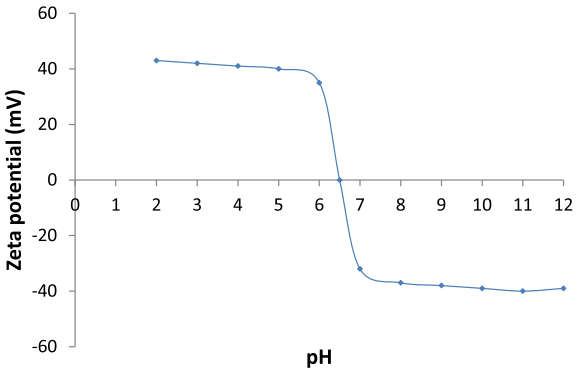

Figure 2. Effect of pH on zeta potential of *P. oceanica* powder in aqueous suspension. (Biomass dose = 3.33 $g{\cdot}L^{-1}$, temperature = 30 ± 2 °C).

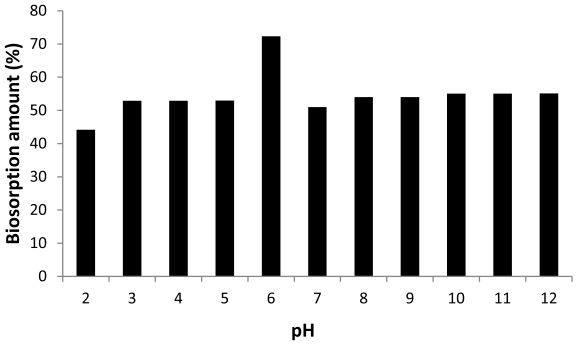

Figure 3. Effect of pH on the nitrate biosorption onto *P. oceanica* powder. (Initial aqueous concentration = 5 mg·L^{-1}, Biomass dose = 3.33 g·L^{-1}, contact time = 60 min, temperature = 30 ± 2 °C).

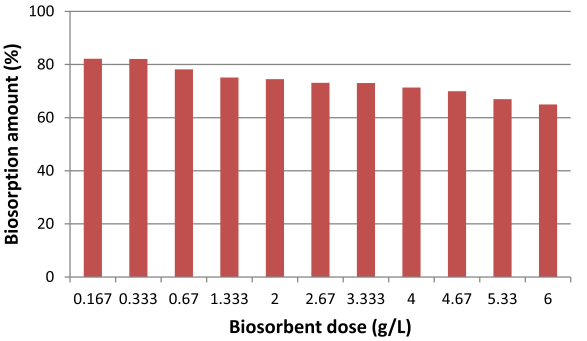

Figure 4. Effect of the biomass dosage on the nitrate biosorption onto *P. oceanica* powder. (Initial aqueous concentration = 5 mg·L^{-1}, pH = 6, contact time = 60 min, temperature = 30 ± 2 °C).

between 3 and 2, the slight decrease of biosorption percentage could be explained by the increase in the number of hydrogen bonds between nitrate and hydronium ions in solution [65]. It can also be ascribed to the partial degradation of cellulose and other polymeric chains in the biosorbent [66].

The second region covers the pH range from 5 to 7 and presents a great increase in biosorption percentage, reaching 72.3% at pH = 6. The ascending part of the curve could be explained by a cooperative effect between two retention modes of nitrate happening simultaneously. The electrostatic interaction with ionized functions and ion exchange with hydroxide ions (OH^-) retained by *P. oceanica* while in seawater and likely during the Section 2.1 step of biosorbent preparation. The cooperative effect between ion exchange and electrostatic interactions to retain nitrate is also confirmed by the zeta potential study. Indeed, at pH = 6, the adsorbent surface is positively charged, and the ion exchange between hydroxide and nitrate can easily take place. The descending part of the curve could be explained by the progressive disappearance of ionized sites, especially $-NH_3^+$ which decreases by about 90% at pH = 7 as described by Navarro et al. [67].

The third region covers the pH range from 7 to 12, showing a nearly constant biosorption percentage with a very small increase toward the most basic media. In this pH region, the nitrate retention is mainly carried out by ion exchange with hydroxide ions. The ion exchange with hydroxide ions was experimentally proven by an increase in the final pH of solutions with initial pH values ranging from 5 to 12. As a result of this study, the optimum pH value chosen was 6, which will be used for all further experiments.

3.1.2. *Effect of biosorbent dosage*

The effect of *P. oceanica* powder dose on the biosorption of nitrate is displayed in Figure 4. The maximum biosorption percentage (82.2%) was found for the lowest biomass dosage (0.167 g·L^{-1}), and subsequently, the biosorption significantly decreases until reaching 65% at 6 g·L^{-1}. It is worth noting that the biosorbent dose used arbitrarily in the study of the pH effects (3.333 g·L^{-1}) corresponds to 73.0%, which is not the optimum value. Figure 4 reveals that this value is located midway between the highest and lowest biosorption percentage values. On the other hand, the decrease in biosorption percentage versus the increasing biosorbent dose, could be explained by the fact that higher concentrations of biomass in suspension can exert a shell effect, thus preventing a good contact between nitrate and available adsorption sites. In fact, the shell effect can be understood by an agglomeration of adsorbent grains on top of each other when they are dispersed at high density in the solution, leading to a remarkable reduction in their specific surface area. As a result, there will not be good contact between the nitrate ions and the active sites of the biosorbent, which leads to a decrease in the percentage of biosorption when the biomass dose exceeds certain

limits. Hence, biosorbent powder exhibits greater nitrate retention at lower dispersion densities than at higher ones. Similar findings were reported and interpreted in previous research works, such as ammonium biosorption by *P. oceanica* [68], orthophosphate biosorption by date palm fibers [69], and heavy metals biosorption by algae [70,71]. As a result of this study, the optimum biosorbent dose was found to be 0.167 g·L^{-1}, which would be used for all further experiments.

3.1.3. *Effect of initial concentrations and contact time*

The effect of initial concentration and contact time on the biosorption of nitrate is displayed in Figure 5. The uptake efficiency is expressed by the amount of nitrate nitrogen biosorbed (Q_e). The experiments were carried out at optimum conditions of pH and biomass dose and at room temperature. All plots in Figure 5 show almost the same trend with three kinetic stages. The first one corresponds to the first 10 min with a rapid increase in the biosorbed amount. In this stage, the fast biosorption can be explained by the existence of a large amount of sorption sites that provide the driving force for faster transfer of the nitrate onto the biosorbent surface as described in a previous work using active carbon to adsorb lead [72]. The second stage covers the range from 10 to 60 min and presents a slow and gradual increase in the biosorbed amount. This can be ascribed to the progressive saturation of sorption sites and the reaching of the equilibrium at the end of this period [72]. The third stage starts from 60 min and presents a saturation plateau corresponding to biosorption equilibrium. Furthermore, raising the nitrate concentration from 5 to 14 mg·L^{-1} of NO_3^-–N, allows the *P. oceanica* powder to increase its biosorption capacity.

Similar findings of the kinetic stages and the effect of initial concentrations were reported for the biosorption of chromium by *P. oceanica* fibers [42]. Thus, the contact time 60 min represents the beginning of the equilibrium state. As a result of this study, the efficiency of biosorption increases with the increase in the initial nitrate concentration, and the optimum contact time is 60 min. It is noted that the optimal contact time coincides with the agitation time chosen arbitrarily in previous experiments (effect of pH and biosorbent dosage), and this time would be used in the following experiments.

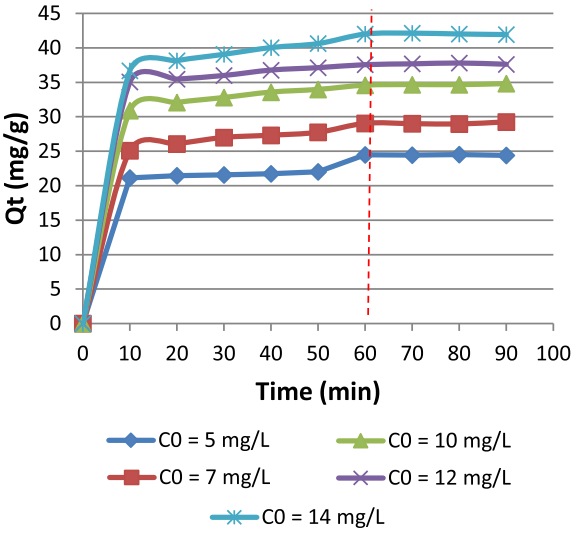

Figure 5. Effect of initial concentrations and contact time on the nitrate biosorption onto *P. oceanica* powder. (pH = 6, Biomass dose = 0.167 g·L^{-1}, temperature = 30 ± 2 °C).

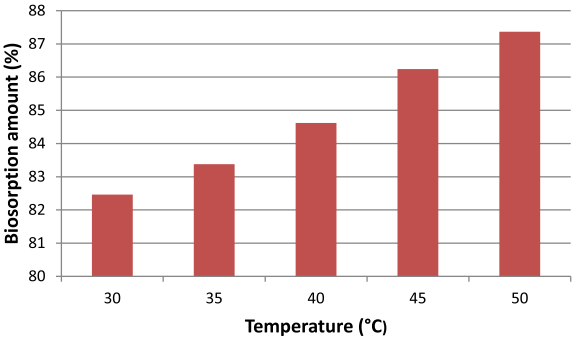

Figure 6. Effect of temperature on the nitrate biosorption onto *P. oceanica* powder. (Initial aqueous concentration = 5 mg·L^{-1}, pH = 6, Biomass dose = 0.167 g·L^{-1}, contact time = 60 min).

3.1.4. *Effect of temperature*

The effect of the temperature on the biosorption of nitrate by *P. oceanica* powder is displayed in Figure 6. This figure shows that the biosorption percentage increases significantly with the increase in temperature, from 82% at 30 °C to 87% at 50 °C. Such a behavior means that biosorption is an endothermic process and any increase in temperature is favorable to nitrate retention by *P. oceanica* powder.

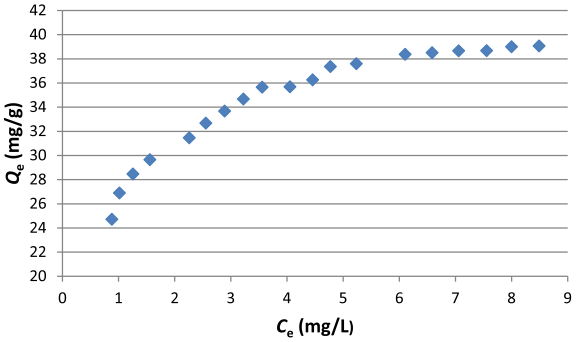

Figure 7. Isotherm of nitrate biosorption onto *P. oceanica* powder. (pH = 6, biomass dose = 0.167 g·L^{-1}, contact time = 60 min, temperature = 30 ± 2 °C).

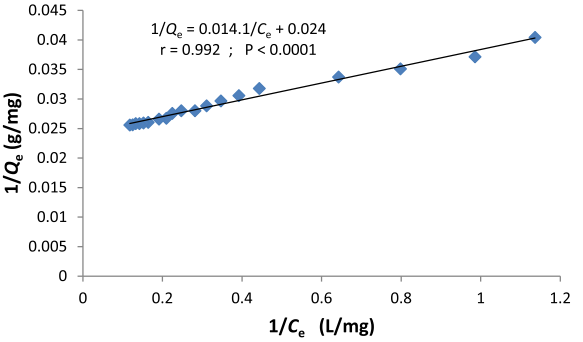

Figure 8. Langmuir linear model of the isotherm of nitrate biosorption onto *P. oceanica* powder. (pH = 6, biomass dose = 0.167 g·L^{-1}, contact time = 60 min, temperature = 30 ± 2 °C).

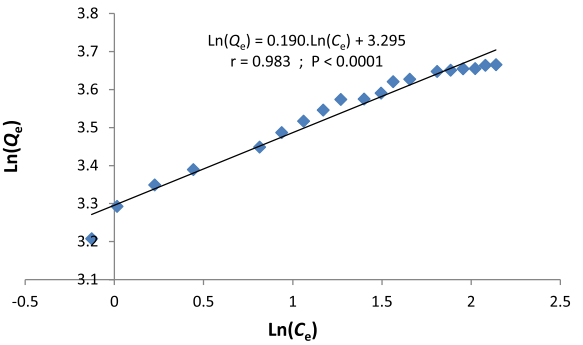

Figure 9. Freundlich linear model of the isotherm of nitrate biosorption onto *P. oceanica* powder. (pH = 6, biomass dose = 0.167 g·L^{-1}, contact time = 60 min, temperature = 30 ± 2 °C).

3.2. *Biosorption isotherms*

The biosorption isotherm was plotted under the optimal conditions of different factors, at room temperature and with initial nitrate concentrations ranging from 5 to 15 mg·L^{-1} of NO_3^- – N with an increment of 0.5 mg·L^{-1} of NO_3^- – N, as presented in Figure 7. The Langmuir linear model applied to this isotherm plotting $1/Q_e$ versus $1/C_e$ indicates a good correlation with the experimental data (r = 0.992) and allows the determination of the maximum biosorption capacity Q_{max} = 41.6 mg·g^{-1} as well as the Langmuir constant b = 1.72 L·mg^{-1} (Figure 8). The equilibrium factor R_L values were estimated from 0.037 to 0.104 depending on initial nitrate concentration. These R_L values are significantly lower than 1 (close to zero), indicating that the biosorption of nitrate by *P. oceanica* powder is highly favorable (and tends toward irreversibility).

In the Freundlich model, the linear plot of Ln(Q_e) versus Ln(C_e) allows for the estimation of the Freundlich constant K_F = 26.98 mg$^{(1-(1/n))}$·L$^{1/n}$·g^{-1} and the value of n = 5.26 (Figure 9). The Freundlich modeling also shows a good correlation with experimental data (r = 0.983) with an n value between 2 and 10, indicating a good biosorption process of nitrate by *P. oceanica* powder.

Figure 10 shows the D–R linear form model allowing the estimation of the maximum biosorption capacity Q_{max} = 75.0 mg·g^{-1} and the activity coefficient $\beta = 2 \cdot 10^{-9}$ mol^2·J^{-2}. The D–R model also shows a good compatibility with experimental data (r = 0.988), and through the β value it allows the calculation of the biosorption mean free energy E = 15.81 kJ·mol^{-1}.

The parameters deduced from the Langmuir, Freundlich, and D–R models are summarized in Table 3.

The Langmuir model has the highest correlation coefficient value (r) and fits better the experimental data. Moreover, although all three models demonstrate good fit with experimental data based on the Chi-square test (Table 4), the Langmuir model exhibits the smallest deviations between observed and theoretical values (smallest value of χ^2_{obs}). Thus, biosorption mainly occurs by a monolayer process on a homogeneous surface with a finite number of

Table 3. Langmuir, Freundlich, and D–R parameters for the biosorption of nitrate onto *P. oceanica* powder

Langmuir			Freundlich			D–R		
b ($L \cdot mg^{-1}$)	Q_{max} ($mg \cdot g^{-1}$)	r	K_F ($mg^{(1-(1/n))} \cdot L^{1/n} \cdot g^{-1}$)	n	r	Q_{max} ($mg \cdot g^{-1}$)	E ($kJ \cdot mol^{-1}$)	r
1.72	41.6	0.992	26.98	5.26	0.983	75.0	15.81	0.988

pH = 6, biomass dose = 0.167 $g \cdot L^{-1}$, contact time = 60 min, temperature = 30 ± 2 °C.

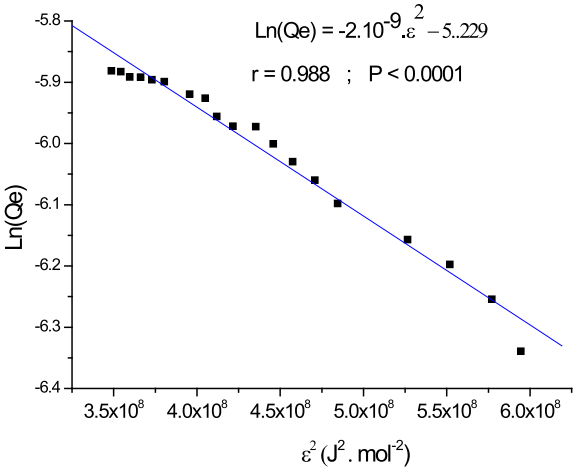

Figure 10. D–R linear model of the isotherm of nitrate biosorption onto *P. oceanica* powder. (pH = 6, biomass dose = 0.167 $g \cdot L^{-1}$, contact time = 60 min, temperature = 30 ± 2 °C).

Table 4. Conformity Chi-square test applied at 95% confidence level to the isotherm models used

Chi-square test	Langmuir	Freundlich	D–R
χ^2_{obs}	0.216	0.369	6.485
χ^2_c	28.869	28.869	28.869
$n-1=18$; $\alpha=0.05$			
Retained hypothesis	H_0	H_0	H_0

identical sites, and no interaction between sorbed nitrate ions. Furthermore, the value of mean free energy, calculated by D–R model, is between 8 and 16 $kJ \cdot mol^{-1}$, substantiating that the nitrate biosorption was conducted by a chemisorption mechanism. In accordance with this mechanism, the nitrate ions were mainly retained by an ion exchange process as suggested in Section 3.1.1 of pH effect. They are also held by ion sharing between aqueous solution and biosorbent surface as mentioned by previous research works using *P. oceanica* to remove ammonium ions [68] and metal-complexed textile dye [73] from aqueous solutions.

Figure 11 displays the Langmuir nonlinear model superposed on the experimental isotherm of nitrate biosorption. It is clearly demonstrated that the Langmuir saturation plateau begins at an equilibrium concentration of 6 $mg \cdot L^{-1}$ of $NO_3^- - N$, corresponding to the initial concentration of 12.5 $mg \cdot L^{-1}$ of $NO_3^- - N$. This initial concentration, in turn, matches 12.5 × 4.428 = 55.35 $mg \cdot L^{-1}$ of NO_3^-. What is worthy to note is that the Langmuir slope is high for concentrations below 55.35 $mg \cdot L^{-1}$ of NO_3^-, and much smaller for those above this threshold. This observation clearly shows that the first biosorption layer is saturated for an initial nitrate concentration of 55.35 $mg \cdot L^{-1}$ and that the additional biosorption of nitrates to form a second layer is practically difficult or very unlikely. It indicates that the *P. oceanica* powder is efficient to treat moderate content nitrate waters, such as most natural waters, potable water, and secondary treated urban wastewater.

Furthermore, based on Langmuir and experimental maximum biosorption capacity (41.6 and 39 mg/g, respectively), the comparison with other nitrate adsorbents in the literature reveals that *P. oceanica* powder is one of the most efficacious nitrate biosorbent (Table 5). This biosorbent also presents more advantages such as being free, widely abundant in Mediterranean coasts, and easily applied without previous preparations. The high value of nitrate uptake by *P. oceanica* powder was reached without the need of any chemical modification or cross-linking with other material as mentioned in many previous

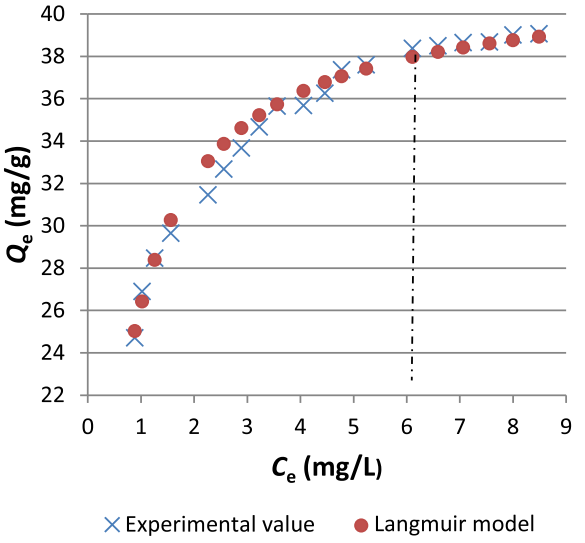

Figure 11. Isotherm and Langmuir non linear model of nitrate biosorption onto *P. oceanica* powder (pH = 6, biomass dose = 0.167 g·L^{-1}, contact time = 60 min, temperature = 30 ± 2 °C).

research works (see Table 5). At full scale, the raw water to be denitrified by *P. oceanica* powder does not require special treatment before or after biosorption, which makes for an easy application and low-cost process. Besides, the biosorbent saturated after use can be incinerated and stocked in confined places far from natural water resources.

The nitrate removal from aqueous media by biosorption onto the dead seagrass *P. oceanica* makes it possible to solve several problems simultaneously in Tunisia. On the one hand, the nitrate removal from drinking water protects public health against several diseases, particularly among infants and vulnerable populations (pregnant women, elderly, etc.). On the other hand, not only does it help clearing coastal areas of massive brown piles of dead *P. oceanica* but it also makes the landscape pleasant for swimming and tourist activities, as well as facilitates the fishing boats mooring and maneuvering in ports. In addition, the nitrate removal in wastewater treatment plants makes it possible to avoid discharging nitrogen-rich water into aquatic media (sea, rivers, or lakes) and, consequently, avoids the phenomenon of eutrophication. The latter risks may lead to an ecological imbalance due to the depletion of dissolved oxygen.

3.3. *Kinetic modeling and biosorption mechanism investigation*

Table 6 displays the calculated coefficients k_1 and $Q_{cal.1}$ for the pseudo-first-order model, k_2 and $Q_{cal.2}$ for the pseudo-second-order model, and k_p for the intraparticle diffusion model, along with the corresponding correlation coefficient (r) for each. For the pseudo-first order model, except for only one value of r (0.995), all the others are relatively low, lying between 0.950 and 0.990. Furthermore, the difference between the calculated and experimental values of nitrate nitrogen amount adsorbed at equilibrium is very high. The error between the experimental and theoretical data ranges from 41 to 85%. As a result, the pseudo-first-order model fits the experimental data poorly and cannot describe the biosorption.

For the pseudo-second-order model, the correlation coefficients for all initial concentrations are extremely high, ranging between 0.997 and 0.999. Moreover, the difference between the calculated and experimental values of nitrate-nitrogen amount adsorbed at equilibrium is minimal (error between 2.1 to 4.5%) (Figure 12). These results reveal a good agreement between the experimental and theoretical data, which means that the biosorption is well described by the pseudo-second-order model. Consequently, biosorption is mainly governed by a chemical process involving ion exchange or anion sharing between nitrate and biosorbent, as described by some previous research works using *P. oceanica* for ammonium [68] and orthophosphate [44] removal.

On the other hand, the plot of intraparticle diffusion model displayed in Figure 13 clearly shows the three stages of mass transfer as mentioned in Section 2.7. For all initial nitrate-nitrogen concentrations, the first stage ($t^{1/2}$ between 0 and 3.1) is characterized by high slope and describes the film diffusion, in which there is transport of nitrate from solution to the exterior surface of the cell membrane of *P. oceanica*. The second stage of the curve, with lower slopes ($t^{1/2}$ between 3.1 and 7.8), represents the intraparticle diffusion, in which nitrate is transported from the extracellular environment into the interior of the cell membrane of *P. oceanica*. The third stage, with null slopes ($t^{1/2} > 7.8$) reflects the equilibrium state of nitrate biosorption. As a result of this analysis, the presence of three distinguished stages in the curves for all initial concentrations and the relatively

Table 5. The maximum adsorption capacity of nitrate by various adsorbents cited in literature

Adsorbent	Q_{max} (mg of nitrate/g) (original unit in the reference)	Q_{max} (mg of nitrate nitrogen/g)	Reference
Zinc chloride ($ZnCl_2$) treated coconut granular activated carbon	Langmuir: 10.26 at 25 °C Langmuir: 10.37 at 10 °C	2.31 2.34	[74]
Activated carbon from pomegranate rind (treated at 300 °C)	Langmuir: 13.10 Langmuir: 11.61	2.96 2.62	[29]
Sugarcane bagasse vermicompost	Langmuir: 15.77 Sips: 17.19	3.56 3.88	[26]
Agriculture waste		Wheat straw charcoal: 1.1 Mustard straw charcoal: 1.30 Commercial activated carbon: 1.22	[27]
Chitosan	Experimental: 19 Langmuir: 8.03 Freundlich: 23.85	4.29 1.81 5.39	[25]
Various materials for nitrate adsorption	Activated carbon: 4.14 Sepiolite: 3.46 Sepiolite activated by HCl: Experimental: 9.80 Langmuir: 38.16	0.93 0.78 2.21 8.61	[30]
Zeolite-supported zero-valent iron nanoparticles	Langmuir: 22.94	5.18	[75]
Local clay	Experimental: 5.10 Langmuir: 27.77	1.15 6.27	[76]
Polyethylene glycol/chitosan composites and polyvinyl alcohol/chitosan composites	(PEG) Langmuir: 35.03 (PVA) Langmuir: 50.68	7.91 11.44	[31]
Activated carbon coated by Fe_3O_4 magnetic nanoparticles	Langmuir: 57.1 at 20 °C Langmuir: 64.5 at 35 °C	12.89 14.56	[32]
Magnetic Co_3O_4/Fe_3O_4 doped polyaniline nanocomposite	Langmuir: 68.96	15.57	[77]
Chitosan hydrogel beads	Langmuir: 92.1	20.80	[78]
Magnetic amine-crosslinked biopolymer	Langmuir: 65.36 at 25 °C Langmuir: 102.04 at 45 °C	14.76 23.04	[33]

(continued on next page)

Table 5. (continued)

Adsorbent	Q_{max} (mg of nitrate/g) (original unit in the reference)	Q_{max} (mg of nitrate nitrogen/g)	Reference
Modified wheat residue	Modified wheat residue: Langmuir: 2.08 (mmol/g) Raw wheat residue Langmuir: 0.02 (mmol/g)	29.12 0.28	[79]
Magnetic zeolite/nanocomposite	Experimental: 421.5 Langmuir: 500	95.2 112.9	[80]
Polymer modified with quaternary ammonium groups	Langmuir: 221.81	50.1	[81]
Carbon	Powdered activated carbon: Langmuir: 10 mmol/g Carbon nanotube: Langmuir: 25 mmol/g	140.0 350.0	[24]
The present work		Experimental: 39 Langmuir: 41.6	

Table 6. Kinetic parameters for the biosorption of nitrate onto *P. oceanica* powder

		Initial nitrate-nitrogen concentration ($mg{\cdot}L^{-1}$)				
		5	7	10	12	14
Experimental Q_e ($mg{\cdot}g^{-1}$)		24.5	29.0	34.8	37.7	42.1
Pseudo-first-order model	k_1 (min^{-1})	0.007	0.028	0.034	0.033	0.033
	$Q_{cal.1}$ ($mg{\cdot}g^{-1}$)	3.6	5.1	20.9	21.8	24.9
	r	0.990	0.995	0.974	0.968	0.950
Pseudo-second-order model	k_2 ($g{\cdot}mg^{-1}{\cdot}min^{-1}$)	0.009	0.010	0.013	0.018	0.009
	$Q_{cal.2}$ ($mg{\cdot}g^{-1}$)	25.6	30.3	35.7	38.5	43.5
	r	0.997	0.999	0.999	0.999	0.999
Intraparticle diffusion	k_p ($mg{\cdot}g^{-1}{\cdot}min^{-0.5}$)	0.210	0.690	0.796	0.554	1.011
	r	0.987	0.991	0.997	0.981	0.998

pH = 6, biomass dose = 0.167 $g{\cdot}L^{-1}$, temperature = 30 ± 2 °C.

high correlation coefficients of the linearized intraparticle diffusion section (r between 0.981 and 0.998; see Table 6) lead to the conclusion that intraparticle diffusion model plays an important role in the nitrate biosorption onto *P. oceanica*.

3.4. *Thermodynamic study*

This study gives insight into the description and estimation of the behavior of the biosorption reaction, such as its spontaneity, thermicity, and the variation introduced on the randomness state in the biosorbent–solution system. The same experimental data used in Section 3.1.4 (temperature effect) were used to calculate ΔG_T^0 at each chosen temperature. The values of ΔH_T^0 and ΔS_T^0 were determined through the slope and intercept of the plot $\mathrm{Ln}(K_C) = f(1/T)$ (Figure 14), respectively. All thermodynamic results are summarized in Table 7.

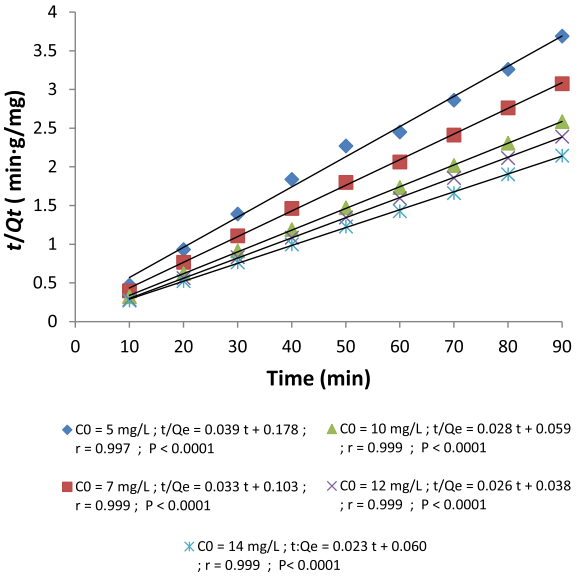

Figure 12. The plots of the pseudo-second-order model of nitrate biosorption onto *P. oceanica* powder. (pH = 6, biomass dose = 0.167 g·L^{-1}, temperature = 30 ± 2 °C).

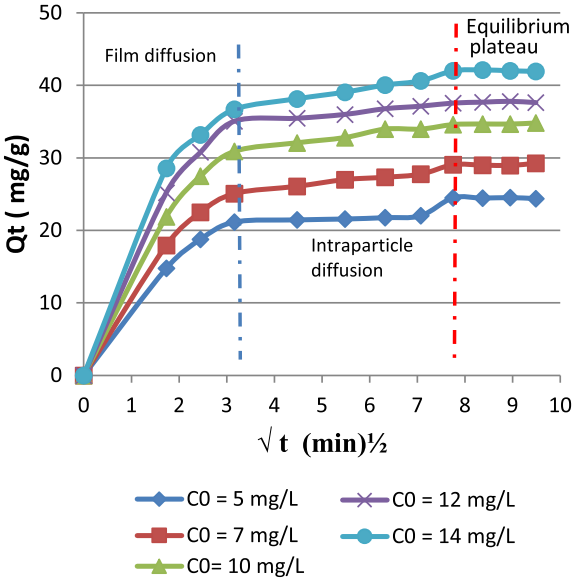

Figure 13. The plots of intraparticle diffusion model of nitrate biosorption onto *P. oceanica* powder. (pH = 6, biomass dose = 0.167 g·L^{-1}, temperature = 30 ± 2 °C).

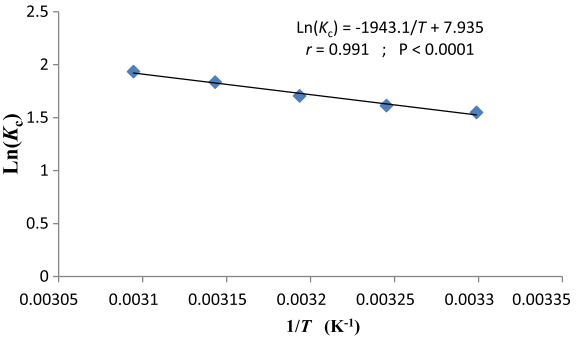

Figure 14. The plot of Ln(K_C) versus 1/T. (Initial aqueous concentration = 5 mg·L^{-1}, pH = 6, biomass dose = 0.167 g·L^{-1}, contact time = 60 min).

Table 7. Thermodynamic parameters for the biosorption of nitrate onto *P. oceanica* powder

T (°C)	K_C	ΔG_T^0 (kJ·mol^{-1})	ΔH_T^0 (kJ·mol^{-1})	ΔS_T^0 (J·mol^{-1}·K^{-1})
30	4.70	−3.90	16.15	65.97
35	5.02	−4.13		
40	5.50	−4.44		
45	6.27	−4.85		
50	6.91	−5.19		

Initial aqueous concentration = 5 mg·L^{-1}, pH = 6, biomass dose = 0.167 g·L^{-1}, contact time = 60 min.

As shown by Table 7 and Figure 14, the negative sign of ΔG_T^0 at all chosen temperatures means that biosorption is spontaneous, whereby no energy input from outside the system is required. The positive value of ΔH_T^0 indicates that the biosorption is endothermic in nature as it was noticed previously (Section 3.1.4). Furthermore, the low value of biosorption heat (ΔH_T^0 < 40 kJ·mol^{-1}) obtained in this work indicates that nitrate was mainly retained by electrostatic interactions and no covalent bond should take place, as described and suggested by a previous research work using chitosan hydrogel beads to remove nitrate from water [78]. The positive value of entropy, in turn, means an increase in the randomness state of the solid–liquid interface after nitrate retention, which indicates some changes occurring in the internal structure of the biosorbent [82].

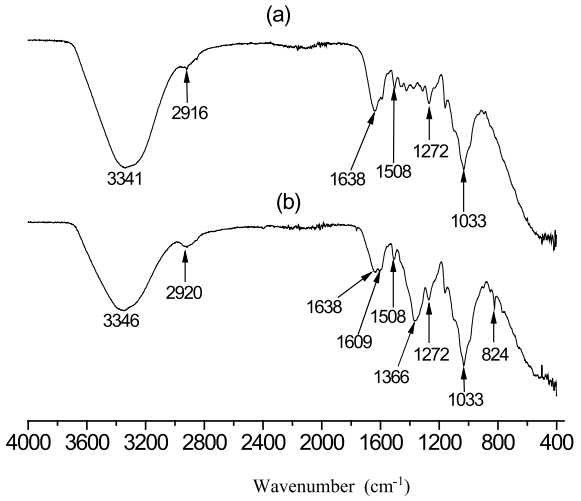

Figure 15. Infrared spectra of *P. oceanica* powder. (a) Native *P. oceanica*; (b) loaded *P. oceanica*–NO_3^-.

3.5. *FTIR characterization*

The aim of infrared characterization is to compare the spectra of *P. oceanica* powder before and after incubation with nitrates to locate the appearance of new bands or the modification in intensity or shape of certain already-existing bands. To this end, attributing bands to functional groups and chemical bonds requires the use of reference work and the infrared correlation chart. Figure 15 shows two superposed spectra of *P. oceanica* before and after nitrate retention.

Since *P. oceanica* is a plant material consisting mainly of cellulose and other less important constituents, such as proteins and lignin, their characteristic bands are clearly visible on both spectra. Indeed, the band around 3340 cm^{-1} can correspond either to the valence vibration of bound –O–H, or to the valence vibrations of –NH in amines emanating from the plant's vegetal proteins [83,84]. The band around 2920 cm^{-1} corresponds to the –C–H alkane valence vibration [85,86], while the band around 1638 cm^{-1} is attributed to the N–H amine deformation vibration [83], as well as the H–O–H valence vibration of the absorbed water [85,86]. The band around 1508 cm^{-1} could correspond to the N–H valence vibration in the amino acids of plant proteins RNH_3^+, $R_2NH_2^+$, and R_3NH^+ as well as the deformation vibration of N–H in primary amines [83]. The bands around 1272 and 1033 cm^{-1} can correspond to the C–O valence vibrations of aryl ether and alkyl ether, respectively. On the spectrum of the loaded *P. oceanica*–NO_3^-, the appearance of new bands provides evidence for the insertion of nitrate ions into the structure of plant fibers. The two bands around 1609 and 1366 cm^{-1} are characteristic of the nitrate ion as shown in a previous study [83]. Indeed, the band around 1609 cm^{-1}, which forms a shoulder with the band at 1638 cm^{-1} by changing its shape, can correspond to the asymmetric valence vibration of the nitro $–NO_2$ group. The band around 1366 cm^{-1} may correspond to the symmetrical valence vibration of the nitro $–NO_2$ group, as illustrated by Scheme 1 (see Section 2.9 in the Material and methods section).

The small new band that appears on the *P. oceanica*–NO_3^- spectrum around 824 cm^{-1} may correspond to the out-of-plane N–H deformation vibration of amines [83]. The appearance of this band could be explained by interactions between nitrates and amines. Given that the nitrate ion can be neither a Lewis acid nor a Lewis base, the hypothesis of its retention through coordination bonds is unlikely to be accepted. It then appears that nitrate ions are retained mainly via electrostatic bonds with charged amines RNH_3^+, $R_2NH_2^+$, and R_3NH^+. The hypothesis of intraparticle retention by the diffusion of nitrates in the cavities of the cellulose crystal lattice can also be considered [87].

3.6. *SEM and EDS characterization*

Figure 16 displays the SEM micrographs of native *P. oceanica* and *P. oceanica*–NO_3^- obtained at 50 and 5 μm magnifications. The micrograph at 50 μm obviously shows the ultimate cellulosic fibers. At this resolution level, while the micrograph of native *P. oceanica* illustrates the condensed and assembled fibers, that of *P. oceanica*–NO_3^- elucidates isolated fibers that are far from each other. These observations can be explained by the insertion of nitrate ions between the fibers and the formation of new electrostatic bonds, including hydrogen bonds and van der Waals forces. These new forces impose a sort of arrangement and orientation of the fibers in well-defined directions [88], and thus the fibers move away from each other. The micrograph at 5 μm shows

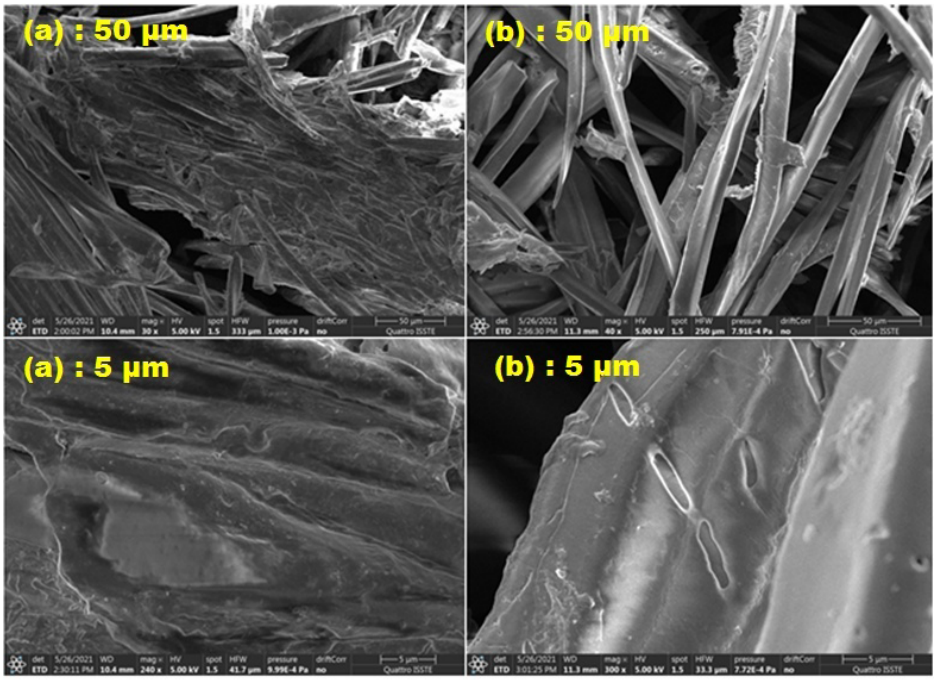

Figure 16. SEM photograph of *P. oceanica* powder before (a) and after nitrate biosorption (b).

the surface of one ultimate cellulosic fiber. At this resolution level, the micrograph of native *P. oceanica* indicates a homogenous surface covered by intact plant matter. However, the micrograph of *P. oceanica*–NO_3^- suggests a degraded and fragmented layer, which supports the hypothesis of chemical structure modification on the fiber surface following interaction with nitrate ions.

Figure 17 shows the EDS spectra (chemical analysis) of native *P. oceanica* and loaded *P. oceanica*–NO_3^-. The spectrum (a) of native *P. oceanica* shows the two significant signals of oxygen and nitrogen, which provides strong evidence not only that nitrogen exists in the chemical structure of the plant biomass as amine groups, but also that oxygen exists as alcohol groups and in the pyranosic rings of cellulosic chains. The spectrum (b) of *P. oceanica*–NO_3^- shows a notable increase in nitrogen and oxygen signals, explained by the insertion of nitrate into the plant's biomass structure. Moreover, it is worth noting that the oxygen signal increases significantly more than that of nitrogen. This observation can be explained by the fact that each incoming nitrate ion introduces one nitrogen atom and three oxygen atoms.

3.7. *Biosorption mechanism*

Understanding the biosorption mechanism is crucial to identifying the chemical groups or ions on the biosorbent surface that are involved in nitrate retention. Kinetic study shows that the biosorption is well described by the pseudo-second-order model rather than the pseudo-first-order one, and the D–R isotherm modeling, in turn, demonstrates that the mean free energy is between 8 and 16 $kJ{\cdot}mol^{-1}$. Together, both results confirm that nitrate was retained by chemisorption [89–92]. In accordance with this, the nitrate ions were mainly retained by an ion exchange process, as observed and described by some previous studies [68,73]. The hypothesis of chemisorption via ion exchange with hydroxide ions was experimentally proven during the pH effect study. In fact, following the biosorption process, the final pH of the aqueous solutions was consistently higher than the initial pH across the range of 5–12. Furthermore, the intraparticle isotherm model reveals good agreement with the experimental data, and its plot clearly displays the three stages upon which its assumptions are based (see Figure 13). This behavior suggests that nitrate

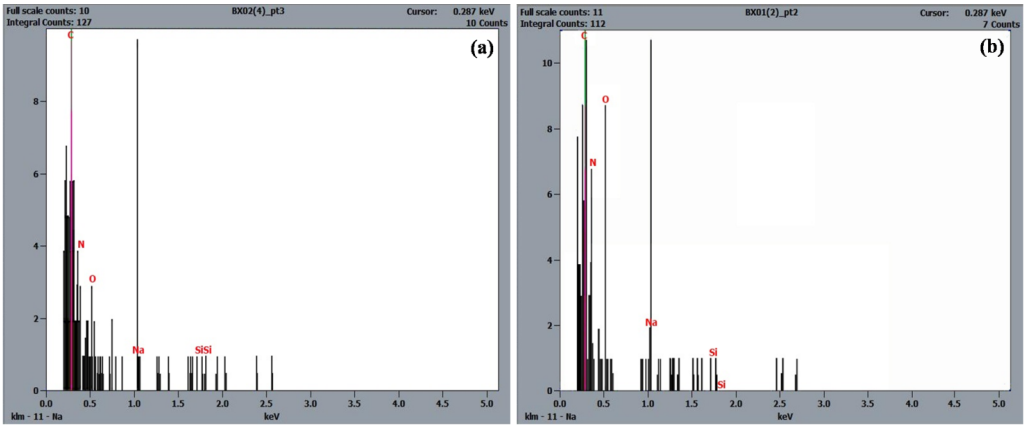

Figure 17. EDS spectra of *P. oceanica* powder before (a) and after nitrate biosorption (b).

retention by intraparticle diffusion may occur, but to a lesser extent than by ion exchange. On the other hand, the analysis of infrared spectra indicates that nitrate may interact through electrostatic forces with the charged amine on the biomass surface (RNH_3^+; $R_2NH_2^+$; R_3NH^+). However, at pH = 6 (optimal value for biosorption), the number of protonated amines on the biosorbent surface is very small, which suggests that this process of nitrate retention is very weak compared to that of ionic exchange. In conclusion, it is estimated that at pH = 6, nitrate retention occurs predominantly through ion exchange, which appears to be the most significant mechanism, while electrostatic interactions and intraparticle diffusion may also occur but play a considerably lesser role.

4. Conclusion

The removal of nitrate from aqueous solutions was performed by biosorption onto abundant sea plant *P. oceanica*. The biosorption was carried out in batch experiments at room temperature and under optimal conditions. It was found that the Langmuir model fit better the experimental data, confirming a monolayer biosorption process onto homogeneous surface and with a finite number of identical active sites. The Langmuir maximum nitrate uptake was found to be equal to 41.6 $mg{\cdot}g^{-1}$ of nitrate nitrogen, showing good efficiency of the biosorbent used. This high value of nitrate uptake by *P. oceanica* powder was reached without the need for any chemical modification or cross-linking with other material as mentioned in many previous research works reported in the literature. The Dubinin–Radushkevich modeling, in turn, gives a mean free energy of 15.81 $kJ{\cdot}mol^{-1}$, illustrating that nitrate was retained through a chemisorption process involving ion exchange or ion sharing between the aqueous solution and the adsorbent surface. The thermodynamic study shows that biosorption is spontaneous, endothermic in nature, and accompanied by an increase in entropy. The spectroscopic characterization by FTIR indicates that nitrate was mainly retained through electrostatic interactions with protonated amines onto the biosorbent surface. This result is further supported by EDS and SEM analyses. Consequently, the sea plant *P. oceanica* demonstrates strong potential as an effective biosorbent for nitrate removal from natural waters, offering a sustainable alternative to conventional denitrification methods.

CRediT authorship contribution statement

Abdelbasset Ben Dkhil: Conceptualization, Methodology, Investigation, Formal Analysis, Writing – original draft.
Haitham Elleuch: Investigation, Vizualisation.
Anissa Somrani: Writing – Review and Editing, Formal Analysis.
Amor Hafiane: Writing – Review and Editing, Project administration.

Declaration of interests

The authors do not work for, advise, own shares in, or receive funds from any organization that could benefit from this article, and have declared no affiliations other than their research organizations.

Funding

The authors would like to thank the Ministry of Higher Education and Scientific Research of Tunisia for financial support of this research work.

References

[1] A. Ben Dekhil, A. Ghorbel and T. Boubacker, "Direct determination of nitrate in natural water by ultraviolet first derivative spectrophotometry", *ACAIJ* **14** (2014), pp. 318–327.

[2] J. A. Camargo, A. Alonso and A. Salamanca, "Nitrate toxicity to aquatic animals: a review with new data for freshwater invertebrates", *Chemosphere* **58** (2005), pp. 1255–1267.

[3] H. Dong, H. Chen, C. Shepsko and A. SenGupta, "Resilient nitrate removal by a biological nitrate-selective ion exchange (BIO-NIX) process", *ACS EST Water* **3** (2023), pp. 2989–2995.

[4] Y.-Z. Han, W.-X. Ji, B.-C. Jiang, et al., "Developing a miniaturized spectrophotometer using 235 and 275 nm UVC-LEDs for fast detection of nitrate in natural water and wastewater effluents", *ACS EST Water* **1** (2021), pp. 2548–2555.

[5] C. C. Hunault, A. C. Lambers, T. T. Mensinga, J. W. Van Isselt, H. P. F. Koppeschaar and J. Meulenbelt, "Effects of sub-chronic nitrate exposure on the thyroidal function in humans", *Toxicol. Lett.* **175** (2007), pp. 64–70.

[6] K. G. Lopez, J. Xiao, C. Crockett, C. Lytle, H. Grubbs and M. Edwards, "Seasonal fluctuation in nitrate levels can trigger lead solder corrosion problems in drinking water", *Environ. Sci. Technol. Lett.* **10** (2023), pp. 21–26.

[7] M. Sadeqa, C. L. Moeb, B. Attarassic, I. Cherkaouid, R. ElAouada and L. Idrissia, "Drinking water nitrate and prevalence of methemoglobinemia among infants and children aged 1–7 years in Moroccan areas", *Int. J. Hyg. Environ. Health* **211** (2008), pp. 546–554.

[8] A. Nasraoui, M. A. Majdoub, M. Hamdaoui and A. Hedhili, "Les nitrates dans les nappes phréatiques du nord tunisien", *Rev. Tun. Biol. Clim.* **19** (2012), pp. 36–40.

[9] L. Fewtrell, "Drinking-water nitrate, methemoglobinemia, and global burden of disease: a discussion", *Environ. Health Prespect.* **112** (2004), pp. 1371–1374.

[10] Ministère de la santé de Tunisie, *Registre des cancers, données 2010–2014*, 2021. Online at https://santetunisie.rns.tn/images/cancersudtunisien2010_2014.pdf (accessed on September 16, 2025). pp. 48-49.

[11] WHO, *Guidelines for Drinking Water Quality, Second Edition, Recommendations*, WHO: Geneva, 1993, pp. 52–53.

[12] U.S. Environmental Protection Agency, *Drinking Water Standards and Health Advisories*, US Environmental Protection Agency, Office of Water: Washington, DC, 2000. 822-B-00-001.

[13] Y. Wu, Y. Wang, J. N. Wang, S. Q. Xu, L. Yu, C. Philippe and T. Wintgens, "Nitrate removal from water by new polymeric adsorbent modified with amino and quaternary ammonium groups: batch and column adsorption study", *J. Taiwan Inst. Chem. Eng.* **66** (2016), pp. 191–199.

[14] A. Bhatnagar and M. Sillanpaa, "A review of emerging adsorbents for nitrate removal from water", *Chem. Eng. J.* **168** (2011), pp. 493–504.

[15] J. A. Camargo and Á. Alonso, "Ecological and toxicological effects of inorganic nitrogen pollution in aquatic ecosystems: a global assessment", *Environ. Int.* **32** (2006), pp. 831–849.

[16] S. Rahdar, K. Pal, L. Mohammadi, A. Rahdar, Y. Goharniya, S. Samani and G. Z. Kyzas, "Response surface methodology for the removal of nitrate ions by adsorption onto copper oxide nanoparticles", *J. Mol. Struct.* **1231** (2021), article no. 129686.

[17] A. O. Rashed, A. M. K. Esawi and A. R. Ramadan, "Novel polysulfone/carbon nanotube polyamide thin film nanocomposite membranes with improved water flux for forward osmosis desalination", *CS Omega* **5** (2020), pp. 14427–14436.

[18] A. Matei and G. Racoviteanu, "Review of the technologies for nitrates removal from water intended for human consumption", *IOP Conf. Ser.: Earth Environ. Sci.* **664** (2021), article no. 012024.

[19] R. M. Garud, S. V. Kore, V. S. Kore and G. S. Kulkarni, "A short review on process and applications of reverse osmosis", *Univers. J. Environ. Res. Technol.* **1** (2011), pp. 233–238.

[20] I. Trus and M. Gomelya, "Low-waste technology of water purification from nitrate on highly basic anion exchange resine", *J. Chem. Technol. Metall.* **57** (2022), pp. 765–772.

[21] S. Duan, T. Tong, S. Zheng, X. Zhang and S. Li, "Achieving low-cost, highly selective nitrate removal with standard anion exchange resin by tuning recycled brine composition", *Water Res.* **173** (2020), article no. 115571.

[22] A. Mohseni-Bandpi, D. J. Elliott and M. A. Zazouli, "Biological nitrate removal processes from drinking water supply-a review", *J. Environ. Health Sci. Eng.* **11** (2013), pp. 1–11.

[23] K. C. Lee and B. E. Rittmann, "Effects of pH and precipitation on autohydrogenotrophic denitrification using the hollow-fiber membrane - biofilm reactor", *Water Res.* **37** (2003), pp. 1551–1556.

[24] A. Bhatnagar and M. Sillanpää, "A review of emerging adsorbents for nitrate removal from water", *J. Chem. Eng.* **168** (2011), pp. 493–504.

[25] M. A. M. Sahli, S. Annouar, M. Mountadar, A. Soufiane and A. Elmidaoui, "Nitrate removal of brackish underground water by chemical adsorption and by electrodialysis", *Desalination* **227** (2008), pp. 327–333.

[26] L. D. Hafshejani, A. Hooshmand, A. A. Naseri, S. A. Mohammadi and F. Abbasi, "Kinetics, isotherm and thermodynamic studies for adsorption of nitrate on sugarcane bagasse vermicompost", *Researcher* **8** (2016), pp. 31–35.

[27] P. C. Mishra and R. K. Patel, "Use of agricultural waste for the removal of nitrate-nitrogen from aqueous medium", *J. Environ. Manag.* **90** (2009), pp. 519–522.

[28] M. Taziki, H. Ahmadzadeh, M. A. Murry and S. R. Lyon, "Nitrate and nitrite removal from wastewater using algae", *Curr. Biotechnol.* **4** (2015), pp. 426–440.

[29] P. C. Mishraa, M. Islama and R. K. Patelb, "Removel of nitrate-nitrogen from aqueous medium by adsorbents derived from pomegranate rind", *Desalin. Water Treat.* **52** (2014), pp. 5673–5680.

[30] N. Öztürk and T. E. Bektaş, "Nitrate removal from aqueous solution by adsorption onto various materials", *J. Hazard. Mater.* **112** (2004), pp. 155–162.

[31] A. Rajeswari, A. Amalraj and A. Pius, "Adsorption studies for the removal of nitrate using chitosan/PEG and chitosan/PVA polymer composites", *J. Water Process Eng.* **9** (2016), pp. 123–134.

[32] R. R. Kalantary, E. Dehghanifard, A. Mohseni-Bandpi, L. Rezaei, A. Esrafili, B. Kakavandi and A. Azari, "Nitrate adsorption by synthetic activated carbon magnetic nanoparticles: kinetics, isotherms and thermodynamic studies", *Desalin. Water Treat.* **57** (2015), pp. 1–11.

[33] W. Song, B. Gao, X. Xu, F. Wang, N. Xue, S. Sun, W. Song and R. Jia, "Adsorption of nitrate from aqueous solution by magnetic amine-crosslinked biopolymer based corn stalk and its chemical regeneration property", *J. Hazard. Mater.* **304** (2016), pp. 280–290.

[34] L. Telesca, A. Belluscio, A. Criscoli, et al., "Seagrass meadows (Posidonia oceanica) distribution and trajectories of change", *Sci. Rep.* **5** (2015), article no. 12505.

[35] E. Balestri, F. Cinelli and C. Lardicci, "Spatial variation is *Posidonia oceanica* structure morphological and dynamic feature in a northwestern Mediterranean coastal area: a multi-scale analysis", *Mar. Ecol. Prog. Ser.* **250** (2003), pp. 51–60.

[36] N. Mayot, C. F. Boudouresque and A. Leriche, "Unexpected response of the seagrass *Posidonia oceanica* to a warm-water in the North Western Mediterranean sea", *C. R. Biol.* **328** (2005), pp. 291–296.

[37] C. F. Boudouresque, A. Jeudy de Grissac and A. Meinesz, "Relation entre la sédimentation et l'allongement des rhizomes orthotrope de *Posidonia oceanica* bans la baie d'Elbu (Corse)", in *International Workshop on Posidonia Oceanica Beds*, GIS Posidonie: Marseille, 1984, pp. 184–191.

[38] N. Cantasano, "The effect of climate changes on *Posidonia oceanic* meadows in the Mediterranean Basin", *NRCR* **6** (2023), pp. 1–6.

[39] C. Lopez y Royo, G. Pergent, T. Alcoverro, et al., "The seagrass *Posidonia oceanica* as indicator of coastal water quality: experimental intercalibration classification systems", *Ecol. Indic.* **11** (2011), pp. 557–563.

[40] B. Akçalı, E. Taşkın, G. Kaman, A. Evcen, H. Çalık and O. Akyo, *Posidonia oceanica Monitoring System on the Coast of Aegean Sea of Turkey*, FUP Best Practice in Scholarly Publishing: Livorno, 2020, pp. 475–482.

[41] M. Montefalcone, "Ecosystem health assessment using the Mediterranean seagrass *Posidonia oceanica*: a review", *Ecol. Indic.* **9** (2009), pp. 595–604.

[42] M. C. Ncibi, B. Majoub, M. Steffen, F. Brouers and S. Gaspard, "Sorption dynamic investigation of chromium (VI) onto *Posidonia oceanica* fibres: kinetic modelling using new generalized fractal equation", *Biochem. Eng. J.* **46** (2009), pp. 141–146.

[43] M. C. Ncibi, B. Majoub and Steffen, "Étude de la biosorption du chrome (VI) par une biomasse méditerranéenne : *Posidonia oceanica* (L.) delile", *Rev. Sci. l'Eau* **21** (2008), pp. 441–449.

[44] M. A. Wahab, R. Ben Hassine and S. Jallali, " *Posidonia oceanica* (L.) fibers as a potential low-coast adsorbent for the removal and recovery of orthophosphate", *J. Hazard. Mater.* **191** (2011), pp. 333–341.

[45] F.-N. Allouche, N. Mameri and G. Eric, "Pb(II) biosorption on Posidonia oceanica biomass", *J. Chem. Eng.* **168** (2011), pp. 1174–1184.

[46] J. Rodier, C. Bazin, J.-P. Broutin, P. Chambon, H. Champsaur and L. Rodi, *L'analyse de L'eau*, 8th edition, Dunod: Paris, 2005, pp. 194–196.

[47] M. I. C. Monterio, F. N. Ferreira, N. M. M. de Oliveira and A. K. Ávila, "Simplified version of the sodium salicylate method for analysis of nitrate in drinking water", *Anal. Chim. Acta* **477** (2003), pp. 125–129.

[48] A. Ben Dekhil and A. Hafiane, "Spectrophotmetric nitrate determination in natural waters by conversion into 4-nitroguaiacol", *Chem. Afr.* **5** (2022), pp. 115–122.

[49] T. Chouchane, M. Yahi, A. Boukari, A. Balaska and S. Chouchane, "Adsorption of the copper in solution by the kaolin", *J. Mater. Environ. Sci.* **7** (2016), pp. 2825–2842.

[50] P.-M. Badot, E. Conte, E. Gravier, P. Bernard-Brunel, B. Fahys and G. Crini, "De l'amidon pour adsorber des colorants", in *Traitement et épuration des eaux industrielles polluées*, 1st edition (G. Crini and P.-M. Badot, eds.), Presses Universitaires de Franche-Comté: Besançon, 2007, pp. 216–217.

[51] K. Kalam, S. A. Abu-Khamsin, M. S. Kamal and S. Patil, "Surfactant adsorption isotherms: a review", *ACS Omega* **6** (2021), pp. 32342–32348.

[52] K. Walsh, S. Mayer, D. Rehmann, T. Hofmann and K. Glas, "Equilibrium data and its analysis with the Freundlich model in the adsorption of arsenic(V) on granular ferric hydroxide", *Sep. Purif. Technol.* **243** (2020), article no. 116704.

[53] M. Chiban, A. Soudani, F. Sinan and M. Persin, "Single? Binary and multi-component adsorption of some anions and heavy metals on environmentally friendly Carpobrotus edulis plant", *Colloids Surf. B: Biointerfaces* **82** (2011), pp. 267–276.

[54] U. R. Malik, S. M. Hasany and M. S. Subhani, "Sorptive potential of sunflower stem for Cr(III) ions from aqueous solutions and its kinetic and thermodynamic profile", *Talanta* **66** (2005), pp. 166–173.

[55] A. Dąqbrowski, "Adsorption - from theory to practice", *Adv. Colloid Interface Sci.* **93** (2001), pp. 135–224.

[56] A. Günay, E. Arslankaya and İ. Tosun, "Lead removal from aqueous solution by natural and pretreated clinoptilolite: adsorption equilibrium and kinetics", *J. Hazard. Mater.* **146** (2007), pp. 362–371.

[57] Y. Hannachi, A. Rezgui, A. Ben Dekhil and T. Boubaker, "Removal of cadmium (II) from aqueous solutions by biosorption onto the brown macroalga (*Dictyota dichotoma*)", *Desalin. Water Treat.* **54** (2015), pp. 1663–1673.

[58] B. Singha, T. K. Naiya, A. K. Bhattacharya and S. K. Das, "Cr(VI) ions removal from aqueous solutions using natural adsorbents-FTIR studies", *J. Environ. Prot.* **2** (2011), pp. 729–735.

[59] M. F. Sawalha, J. R. Peralta-Videa, J. Romero-González, M. Duarte-Gardea and J. L. Gardea-Torresdey, "Thermodynamic and isotherm studies of the biosorption of Cu(II), Pb(II), and Zn(II) by leaves of saltbush (Atriplex canescens)", *J. Chem. Thermodyn.* **39** (2007), pp. 488–492.

[60] Q. Hu and Z. Zhang, "Application of Dubinin–Radushkevich isotherm model at the solid/solution interface: a theoretical analysis", *J. Mol. Liq.* **277** (2019), pp. 646–648.

[61] Y.-S. Ho, "Citation review of Lagergren kinetic rate equation on adsorption reactions", *Scientometrics* **59** (2004), pp. 171–177.

[62] Y. S. Ho and G. McKay, "Pseudo-second order model for sorption processes", *Process Biochem.* **34** (1999), pp. 451–465.

[63] W. J. Weber and J. C. Morris, "Kinetics of adsorption on carbon from solutions", *J. Sanit. Eng. Div., Am. Soc. Civ. Eng.* **89** (1963), pp. 31–60.

[64] R. Aravindhan, J. R. Rao and B. U. Nair, "Removal of basic yellow dye from aqueous solution by sorption on green alga *Caulerpa scalpelliformis*", *J. Hazard. Mater.* **142** (2007), pp. 68–76.

[65] I. Bernal, "The composition, charge and architecture of hydronium ions as observed in the crystalline state", *C. R. Chim.* **9** (2006), pp. 1454–1466.

[66] M. Ioelovich, "Study on acidic degradation of cellulose", *ICMS* **7** (2017), pp. 1–4.

[67] R. Navarro, J. Guzmán, I. Saucedo, J. Revilla and E. Eric Guibal, "Recovery of metal ions by chitosan sorption mechanisms and influence of metal speciation", *Macromol. Biosci.* **3** (2003), pp. 552–561.

[68] S. Jellali, M. A. Wahab, M. Anane, K. Riahi and N. Jedidi, "Biosorption characteristic of ammonium from aqueous solutions onto *Posidonia Oceanica* (L.) fibers", *Desalination* **270** (2011), pp. 40–49.

[69] K. Riahi, K. B. Ben Thayer, A. Ben Mammou, A. Ben ammar and M. H. Jaafoura, "Biosorption characteristics of phosphates from aqueous solution onto *Phoenix dactylifera* L. date palm fibers", *J. Hazard. Mater.* **161** (2009), pp. 608–613.

[70] S. K. Mehta and J. P. Gaur, "Use of algae for removing heavy metal ions from wastewater: progress and prospects", *Crit. Rev. Biotechnol.* **25** (2005), pp. 113–152.

[71] A. Ben Dekhil, Y. Hannachi, A. Ghorbel and T. Boubaker, "Removel of lead and cadmium ions from aqueous solutions using dried marine green macroalgea (Caulerpa racemosa)", *Int. J. Environ. Res.* **5** (2011), pp. 725–732.

[72] A. A. Pama, A. Abdullaha, Y. P. Tana and Z. Zainalb, "Pb(II) removal from wastewater by modified activated carbon in batch and fixed-bed column studies: synthetic and real wastewater application", *Desalin. Water Treat.* **140** (2019), pp. 290–301.

[73] M. C. Ncibi, B. Mahjoub and M. Seffen, "Investigation of the sorption mechanisms of metal-complexed dye onto *Posidonia oceanica* (L.) fibres through kinetic modelling analysis", *Bioresour. Technol.* **99** (2008), pp. 5582–5589.

[74] A. Bhatnagar, J. Minkyu, Y.-H. Choi, et al., "Removel of nitrate from water by adsorption onto zinc chloride treated activated carbon", *Sep. Sci. Technol.* **43** (2008), pp. 886–907.

[75] S. Sepehri, M. Heidarpour and J. Abedi-Koupai, "Nitrate removal from aqueous solution using natural zeolite-supported zero-valent iron nanoparticles", *Soil Water Res.* **9** (2014), pp. 224–232.

[76] A. Battas, A. El Gaidoumi, A. Ksakas and A. Kherbeche, "Adsorption study for the removal of nitrate from water using local clay", *Sci. World J.* **2019** (2019), article no. 9529618.

[77] M. E. Bidhendi, Z. Asadi, A. Bozorgian, A. Shahhoseini, M. A. Gabris, S. Shahabuddin, R. Khanam and R. Saidur, "New magnetic Co_3O_4/Fe_3O_4 doped polyaniline nanocomposite for the effective and rapid removal of nitrate ions from ground water samples", *Environ. Prog. Sustain. Energy* **39** (2019), article no. 13306.

[78] S. Chatterjee and S. H. Seung Han Woo, "The removal of nitrate from aqueous solutions by chitosan hydrogel beads", *J. Hazard. Mater.* **164** (2009), pp. 1012–1018.

[79] Y. Wang, B.-y. Gao, W.-W. Yue and Q.-Y. Yue, "Adsorption kinetics of nitrate from aqueous solutions onto modified wheat residue", *Colloids Surf. A: Physicochem. Eng. Asp.* **308** (2007), pp. 1–5.

[80] E. Darezereshki, F. Bakhtiari and M. Rahmani, "Adsorption removal of nitrate by a novel magnetic zeolite adsorbent (zeolite/γ-Fe_2O_3 nanocomposite) in solution", *Nanotechnol. Environ. Eng.* **8** (2022), pp. 153–166.

[81] W. Yan, W. Yi, W. Jinnan, X. Suqian, Y. Liang, C. Philippe and T. Wintgens, "Nitrate removal from water by new polymeric adsorbent modified with amino and quaternary ammonium groups: Batch and column adsorption study", *J. Taiwan Inst. Chem. Eng.* **66** (2016), pp. 191–199.

[82] S. Dey, S. R. Basha, G. V. Babu and T. Nagendra, "Characteristic and biosorption capacities of orange peels biosorbents for removal of ammonia and nitrate from contaminated water", *Clean. Mater.* **1** (2021), article no. 100001.

[83] D. Pavia, M. Lampman and G. Kriz, *Introduction to Spectroscopy*, 3rd edition, Thomson Learning Publisher: Washigton, 2001, pp. 74–80.

[84] V. K. Jha, Y. Kameshima, A. Nakajima and K. Okada, "Utilization of steel-making slag for the uptake of ammonium and phosphate ions from aqueous solution", *J. Hazard. Mater.* **156** (2008), pp. 156–162.

[85] J. Brandrup and E. H. Immergut, *Polymer Handbook*, 3rd edition, Wiley-Interscience: New York, 1989, p. 117.

[86] L. Ilharco, M. Garcia and R. Lopes, "Infrared approach to the study of adsorption on cellulose: influence of cellulose crystallinity on the adsorption of benzophenone", *Langmuir* **13** (1997), pp. 4126–4132.

[87] Y. Nishiyama, J. Sugiyama, H. Chanzy and P. Langan, "Crystal structure and hydrogen bonding system in cellulose I(alpha) from synchrotron X-ray and neutron fiber diffraction", *J. Am. Chem. Soc.* **125** (2003), pp. 14300–14306.

[88] C. M. Altaner, L. H. Thomas, A. N. Fernandez and M. C. Jarvis, "How cellulose stretches: synergism between covalent and hydrogen bonding", *Biomacromolecules* **15** (2014), pp. 791–798.

[89] R. S. Moussa, O. S. Mamane, I. Habou, M. M. M. Alma and I. Natatou, "Kinetic, isothermal and thermodynamic modeling of fluoride ion adsorption by raw and activated clays", *GSCARR* **14** (2023), pp. 160–173.

[90] A. N. Ebelegi, N. Ayawei and D. Wankasi, "Interpretation of adsorption thermodynamics and kinetics", *Open J. Phys. Chem.* **10** (2020), pp. 166–182.

[91] E. F. Olasehinde, S. M. Abegunde and M. A. Adebayo, "Adsorption isotherms, kinetics and thermodynamic studies of methylene blue dye removal using Raphia taedigera seed activated carbon", *Caspian J. Environ. Sci.* **18** (2020), pp. 329–344.

[92] Q. Hu and Z. Zhang, "Application of Dubinin–Radushkevich isotherm model at the solid/solution interface: a theoretical analysis", *J. Mol. Liq.* **277** (2019), pp. 646–648.